Protein Film Voltammetry of *Rhodobacter Capsulatus* Xanthine Dehydrogenase

Kondo François Aguey-Zinsou,[†] Paul V. Bernhardt,[*,†] and Silke Leimkühler[‡]

Contribution from the Centre for Metals in Biology, Department of Chemistry, University of Queensland, Brisbane 4072, Australia, and Department of Plant Biology, Technical University of Braunschweig, 38023 Braunschweig, Germany

Received August 14, 2003; E-mail: p.bernhardt@uq.edu.au

Abstract: Xanthine dehydrogenase (XDH) from the bacterium *Rhodobacter capsulatus* catalyzes the hydroxylation of xanthine to uric acid with NAD^+ as the electron acceptor. *R. capsulatus* XDH forms an $(\alpha\beta)_2$ heterotetramer and is highly homologous to homodimeric eukaryotic XDHs. The crystal structures of bovine XDH and *R. capsulatus* XDH showed that the two proteins have highly similar folds; however, *R. capsulatus* XDH is at least 5 times more active than bovine XDH and, unlike mammalian XDH, does not undergo the conversion to the oxidase form. Here we demonstrate electrocatalytic activity of the recombinant enzyme, expressed in *Escherichia coli*, while immobilized on an edge plane pyrolytic graphite working electrode. Furthermore, we have determined all redox potentials of the four cofactors ($Mo^{VI/V}$, $Mo^{V/IV}$, FAD/FADH, $FADH/FADH_2$ and two distinct $[2Fe-2S]^{2+/+}$ clusters) using a combination of potentiometric and voltammetric methods. A novel feature identified in catalytic voltammetry of XDH concerns the potential for the onset of catalysis (ca. 400 mV), which is at least 600 mV more positive than that of the highest potential cofactor. This unusual observation is explained on the basis of a pterin-associated oxidative switch during voltammetry that precedes catalysis.

Introduction

The mononuclear Mo-containing enzymes represent a large class of proteins comprising a single Mo ion coordinated by either one or two pyranopterin-dithiolene ligands (also known as molybdopterin).[1] These enzymes are classified into three families[2] according to the number and type of ligands bound to the Mo center; namely, the xanthine oxidase, sulfite oxidase, and dimethyl sulfoxide reductase families (Chart 1).

The xanthine oxidase family comprises a coherent group of enzymes found in all forms of life, usually catalyzing the oxidative hydroxylation of a vast array of heterocyclic compounds including pyridines, purines, pteridines, and pyrazolopyrimidines, in addition to various aromatic and aliphatic aldehydes. The most studied enzyme from this family is xanthine oxidoreductase,[3] comprising xanthine oxidase (XO) and xanthine dehydrogenase (XDH). The mammalian enzyme is synthesized as the dehydrogenase form and exists mostly as such in the cell. However, it can readily be converted to the oxidase form by oxidation of sulfhydryl residues or by proteolysis. Mammalian XDH shows a preference for NAD^+ reduction (although it also reacts with O_2), whereas XO fails to react with NAD^+ and exclusively uses dioxygen as its substrate, leading to the formation of superoxide anion radicals and hydrogen peroxide.[4,5]

Recent crystallographic work on the bovine oxidoreductase has highlighted important structural differences between the two forms, particularly at the putative NAD^+ binding site.[6] Specifically, it has been shown that during the conversion of XDH to XO a major structural rearrangement blocks the access of the NAD^+ substrate to the FAD cofactor and changes the electrostatic environment of the active site, reflecting the switch of substrate specificity observed for the two forms of this enzyme.

The enzyme is a target of drugs against gout and hyperuricaemia, and the conversion of XDH to XO is of major medical interest as it has been implicated in diseases characterized by oxygen-radical-induced tissue damage, such as postischaemic reperfusion injury.[7] In addition, XDH and XO are involved in xanthinuria,[8] drug metabolism,[9] and other conditions such as hepatitis, cancer, and inflammatory disorders.[10] Like most other members of its family, XDH/XO comprises four redox active cofactors: a five-coordinate mononuclear Mo ion (Chart 1), two [2Fe-2S] clusters, and a flavin adenine dinucleotide (FAD) group. The X-ray crystal structures of XDH from bovine milk[6] and from the bacterium *Rhodobacter capsulatus*[11] in addition to the related aldehyde oxidoreductase from *De-*
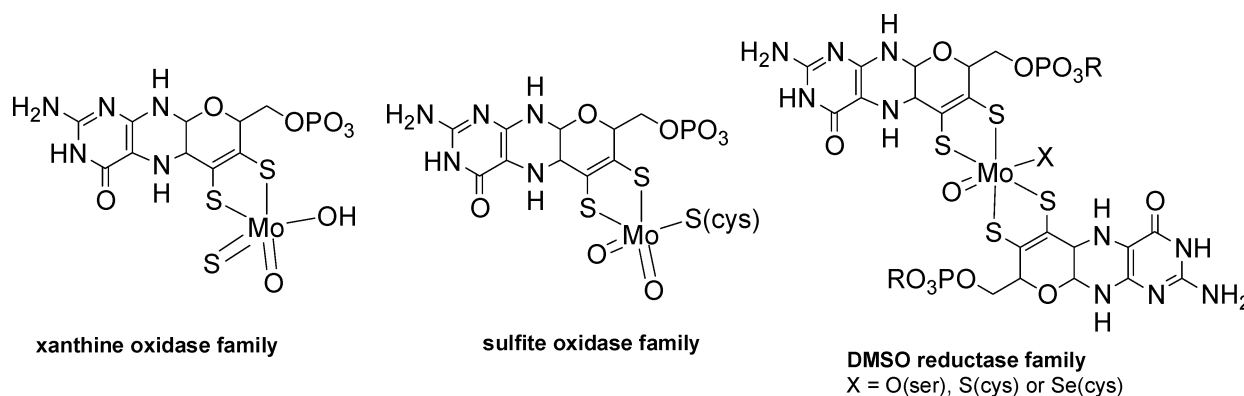
† University of Queensland
‡ Technical Univerisity of Braunschweig.
(1) Hille, R. *Met. Ions Biol. Syst.* **2002**, *39*, 187−226.
(2) Hille, R. *Chem. Rev.* **1996**, *96*, 2757−2816.
(3) Hille, R.; Nishino, T. *FASEB J.* **1995**, *9*, 995−1003.
(4) Nishino, T. *J. Biochemistry (Tokyo)* **1994**, *116*, 1−6.
(5) McManaman, J. L.; Bain, D. L. *J. Biol. Chem.* **2002**, *277*, 21261−21268.

(6) Enroth, C.; Eger, B. T.; Okamoto, K.; Nishino, T.; Nishino, T.; Pai, E. F. *Proc. Natl. Acad. Sci. U.S.A.* **2000**, *97*, 10723−10728.
(7) Harrison, R. *Free Rad. Biol. Med.* **2002**, *33*, 774−797.
(8) Simmonds, H. A.; Reiter, S.; Nishino, T. *The Metabolic and Molecular Bases of Inherited Disease*, 7th ed.; McGraw-Hill Inc.: New York, 1995.
(9) Beedham, C. *Biomed. Health Res.* **1998**, *25*, 39−52.
(10) Borges, F.; Fernandes, E.; Roleira, F. *Curr. Med. Chem.* **2002**, *9*, 195−217.
(11) Truglio, J. J.; Theis, K.; Leimkühler, S.; Rappa, R.; Rajagopalan, K. V.; Kisker, C. *Structure* **2002**, *10*, 115−125.

Chart 1

xanthine oxidase family   sulfite oxidase family

DMSO reductase family
X = O(ser), S(cys) or Se(cys)

sulfovibrio gigas[12] have contributed significantly to our understanding of the function of these enzymes.

Although the electron-transfer properties of XDH and XO have attracted much attention, these studies have been dominated by equilibrium (potentiometric) measurements of the redox centers[13-20] and rapid kinetic experiments[21-27] on electron transfer between the various cofactors. Protein voltammetry provides simultaneous thermodynamic and kinetic information on both reduction potentials and catalytic activity, and there has been considerable activity in this area in the last 10 years.[28] Curiously, the first direct voltammetric responses from a Mo cofactor (in the absence of catalysis) appeared only recently, for the enzymes DMSO reductase[29] and sulfite dehydrogenase.[30] Considering the longstanding interest in the biochemistry of XDH/XO, it is surprising that the protein film voltammetry of XDH/XO has received little attention. The sole report of this type concerned the cyclic voltammetry of bovine milk XO, where a response only from the FAD cofactor could be seen, and the electrochemistry was complicated by denaturation and specific interactions between cysteine residues and Hg working electrode.[31] Furthermore, no direct electrocatalytic activity of the enzyme was demonstrated. In this work, we report the electrochemical characterization of *R. capsulatus* XDH using a combination of EPR potentiometry and protein film voltammetry. In addition to quantifying all six oxidation—reduction couples within the enzyme, we demonstrate pronounced electrocatalytic oxidation of xanthine and at the same time have identified what we believe to be a unique potential-dependent switch of catalytic activity associated with a ligand-centered oxidation at the Mo active site.

Experimental Section

All reagents were obtained commercially and were of analytical grade purity.

Enzyme Preparation. Active *R. capsulatus* XDH in addition to de-Moco XDH was purified after heterologous expression in *E. coli* as previously described.[32]

Cyclic Voltammetry. Voltammetry was performed with a BAS 100B/W electrochemical workstation employing an edge-plane pyrolytic graphite working electrode, an Ag/AgCl reference electrode (+196 mV vs NHE), and a Pt counter electrode. Measurements were performed in an argon-purged 500 μL Tris buffer (50 μM) solution at pH 8 with 0.01 M NaCl as supporting electrolyte, or for pH-variable experiments, in a buffer mixture of bis-tris propane (20mM) and 2-amino-2-methylpropan-1-ol (20 mM) titrated with the appropriate amount of HCl to give a final pH within the range 5 to 10. The concentration of the enzyme was 10 μM in all experiments. The electrode surface was cleaned by cleaving several 1 μm layers from the face of the electrode with a microtome followed by sonication in MilliQ water. No abrasives were used. No other electrode surface conditioning was necessary and no promoters were used. A stable protein film was established within 10 min of immersion of the electrode in the electrochemical cell. The surface coverage of XDH was determined by standard procedures from the gradient of the plot of peak current as a function of scan rate.[33] For catalysis, the cyclic voltammetric peak current (i_{lim}) was determined at various concentrations of xanthine and pH, and the data analysis was as described.[30] At high substrate concentrations ($\gg K_M$) a sigmoidal, steady-state response was observed, whereas at low substrate concentrations a peak current was seen, which is indicative of diffusion-limited substrate depletion. All potentials are cited vs the normal hydrogen electrode.

(12) Romão, M. J.; Archer, M.; Moura, I.; Moura, J. J. G.; LeGall, J.; Engh, R.; Schneider, M.; Hof, P.; Huber, R. *Science* **1995**, *270*, 1170−1176.
(13) Cammack, R.; Barber, M. J.; Bray, R. C. *Biochem. J.* **1976**, *157*, 469−478.
(14) Barber, M. J.; Bray, R. C.; Cammack, R.; Coughlan, M. P. *Biochem. J.* **1977**, *163*, 279−289.
(15) Barber, M. J.; Coughlan, M. P.; Kanda, M.; Rajagopalan, K. V. *Arch. Biochem. Biophys.* **1980**, *201*, 468−475.
(16) Barber, M. J.; Coughlan, M. P.; Rajagopalan, K. V.; Siegel, L. M. *Dev. Biochem.* **1982**, *21*, 805−809.
(17) Barber, M. J.; Siegel, L. M. *Biochemistry* **1982**, *21*, 1638−1647.
(18) Porras, A. G.; Palmer, G. *J. Biol. Chem.* **1982**, *257*, 11617−11626.
(19) Hunt, J.; Massey, V.; Dunham, W. R.; Sands, R. H. *J. Biol. Chem.* **1993**, *268*, 18685−18691.
(20) Parschat, K.; Canne, C.; Huttermann, J.; Kappl, R.; Fetzner, S. *Biochim. Biophys. Acta* **2001**, *1544*, 151−165.
(21) Barber, M. J.; Bray, R. C.; Lowe, D. J.; Coughlan, M. P. *Biochem. J.* **1976**, *153*, 297−307.
(22) Fhaolain, I. N.; Hynes, M. J.; Coughlan, M. P. *Biochem. J.* **1978**, *171*, 83−88.
(23) Bhattacharyya, A.; Tollin, G.; Davis, M.; Edmondson, D. E. *Biochemistry* **1983**, *22*, 5270−5279.
(24) Hille, R.; Massey, V. *J. Biol. Chem.* **1986**, *261*, 1241−1247.
(25) Schopfer, L. M.; Massey, V.; Nishino, T. *J. Biol. Chem.* **1988**, *263*, 13528−13538.
(26) Hille, R. *Biochemistry* **1991**, *30*, 8522−8529.
(27) Walker, M. C.; Hazzard, J. T.; Tollin, G.; Edmondson, D. E. *Biochemistry* **1991**, *30*, 5912−5917.
(28) Armstrong, F. A.; Wilson, G. S. *Electrochim. Acta* **2000**, *45*, 2623−2645.
(29) Aguey-Zinsou, K.-F.; Bernhardt, P. V.; McEwan, A. G.; Ridge, J. P. *J. Biol. Inorg. Chem.* **2002**, *7*, 879−883.
(30) Aguey-Zinsou, K.-F.; Bernhardt, P. V.; Kappler, U.; McEwan, A. G. *J. Am. Chem. Soc.* **2003**, *125*, 530−535.
(31) Rodrigues, C. G.; Wedd, A. G.; Bond, A. M. *J. Electroanal. Chem. Interfacial Electrochem.* **1991**, *312*, 131−140.
(32) Leimkühler, S.; Hodson, R.; George, G. N.; Rajagopalan, K. V. *J. Biol. Chem.* **2003**, *278*, 20802−20811.
(33) Bard, A. J.; Faulkner, L. R. *Electrochemical Methods: Fundamentals and Applications*, 2nd ed.; Wiley: New York, 2001.

Potentiometry. FAD-, [2Fe-2S]- and Mo-based redox potentials were determined by standard redox potentiometry[34] employing EPR spectrometry as the detection method and fitting the appropriate spectroscopic signal intensity to the Nernst equation. Titrations were performed within a Belle Technology glovebox under an atmosphere of N_2 (concentration of $O_2 < 2$ ppm) at 25 °C. The mediators used were 2-hydroxy-1,4-naphthoquinone (8 μM), benzyl viologen (2 μM), and methyl viologen (2 μM), the reductant was $Na_2S_2O_4$, and the oxidant was $K_3[Fe(CN)_6]$. Optical potentiometry employed 6 μM enzyme solution buffered at pH 8 with Tris (50 μM). The solution potential at equilibrium was measured with an ABB Kent Taylor combination Pt−Ag/AgCl electrode attached to a Hanna 8417 meter. Potentials are again cited vs NHE.

For EPR potentiometry, 200 μM samples of XDH (pH 8.0) poised at different redox potentials (within a glovebox) were sealed and frozen in 3 mm diameter quartz tubes using liquid nitrogen. X-band ($\sim$9.3 GHz) continuous wave EPR spectra were recorded on a Bruker Biospin Elexsys E500 EPR spectrometer fitted with a super high Q cavity. Calibration of the magnetic field and microwave frequency for the Elexsys E500 were achieved with a Bruker ER035M Gaussmeter and an EIP 548B microwave frequency counter, respectively. A flow-through cryostat in conjunction with a Eurotherm (B-VT-2000) variable temperature controller provided temperatures between 2 and 140 K at the sample position in the cavity. Spectrometer (Elexys E500) tuning, signal averaging, and subsequent spectral comparisons and plotting were performed with Bruker's Xepr (version 2.1) software. UV−visible measurements were made (within the glovebox) with a Shimadzu UV Mini 1240 spectrophotometer.

Results

Cofactor Redox Potentials. A. Potentiometry. XDH in its fully oxidized state is capable of accepting six electrons. The relevant redox couples are FAD(quinone)/FADH(semiquinone), FADH/FADH$_2$(hydroquinone), Mo$^{VI/V}$, Mo$^{V/IV}$, and two different [2Fe-2S]$^{2+/+}$ centers, commonly referred to as FeSI and FeSII. Previous potentiometric and microcoulometric studies of various XDH[14,15,19,20] and XO[13,18,35,36] enzymes have found that these six redox potentials invariably lie within a relatively narrow range of ca. −200 to −400 mV vs NHE.

In its fully oxidized state, the FAD and [2Fe-2S]$^{2+}$ clusters dominate the visible spectrum of XDH (Figure 1) and the electronic maxima of these chromophores overlap significantly.[37] The absorption maximum for *R. capsulatus* XDH appears at 465 nm, which is somewhat red-shifted compared to the spectrum of bovine XO. This difference is probably due to different environments of FAD in *R. capsulatus* XDH and bovine XO. One-electron reduction to the semiquinone gives rise to a new shoulder at 600 nm (Figure 1), with a concomitant decrease in 465 nm absorption. Further reduction to the hydroquinone is accompanied by disappearance of both the 465 and 600 nm bands. The initial drop in the 465 nm absorbance at higher potentials (above −300 mV, Figure 1) is not matched
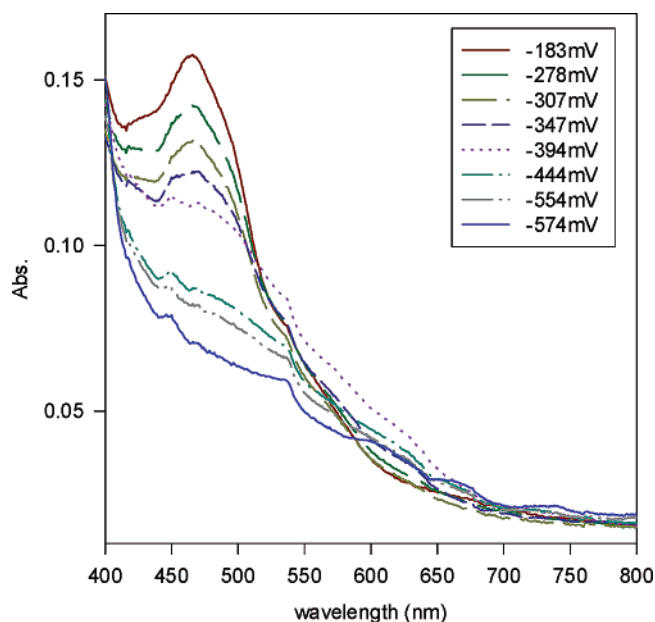

Figure 1. Electronic spectra of XDH (6 μM, pH 8.0) as a function of solution potential. See Experimental Section for other details.
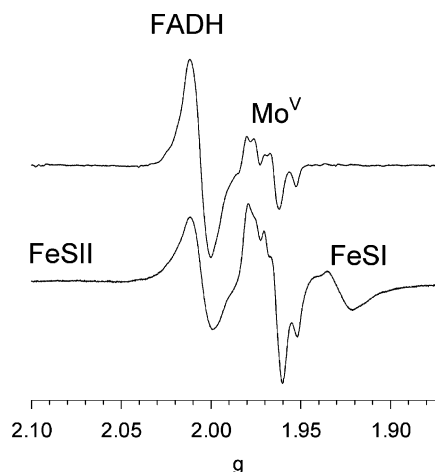

Figure 2. EPR spectra of XDH at 120 K (upper trace, potential −530 mV, $\nu = 9.446$ GHz) and 2K (lower trace, −400 mV, $\nu = 9.358$ GHz). Selected signals from each paramagnetic center are marked.

by a rise in the semiquinone absorbance; thus spectral changes in this region of the titration are due solely to the higher potential [2Fe-2S]$^{2+}$ center. However, beyond this point in the titration, there is overlap of the spectral changes associated with the two 2Fe-2S centers and the FAD cofactor, so analysis of the spectra is difficult, particularly in terms of determining the cofactor redox potentials.

EPR spectroscopy offers superior resolution of the signals from the FAD, 2Fe-2S, and Mo centers. The FADH semiquinone gives an intense isotropic EPR signal at g 2.005 and is easily seen at 120 K (Figure 2, upper trace, potential poised at −530 mV). The entire set of potential-dependent spectra is given in the Supporting Information (Figure S1). The Mo^V-EPR signal is also clearly observed at this temperature. The rhombic Mo spectrum ($g_{1,2,3}$ = 1.950, 1.963, and 1.977) is characteristic of enzymes of the XO family, and spectra of this form have been designated "rapid" type I, with hyperfine coupling to two inequivalent protons, provided by a pair of *cis*-coordinated SH$^-$ and OH$^-$ ligands coordinated to the Mo^V ion.[21] Signals from

(34) Dutton, P. L. *Methods Enzymol.* **1978**, *54*, 411−435.
(35) Spence, J. T.; Barber, M. J.; Siegel, L. M. *Biochemistry* **1982**, *21*, 1656−1661.
(36) Kay, C. J.; Barber, M. J. *Anal. Biochem.* **1989**, *184*, 11−15.
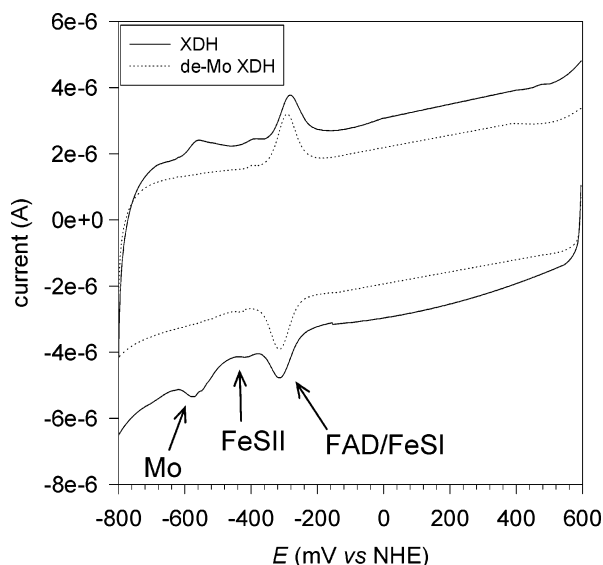(37) Ryan, M. G.; Ratnam, K.; Hille, R. *J. Biol. Chem.* **1995**, *270*, 19209−19212.

Figure 3. Cyclic voltammograms of XDH (solid curve) and de-Moco XDH (dotted curve) (scan rate 50 mV s^{-1}, pH 8.0, 25 °C).

Figure 4. Cyclic voltammetry of XDH in the presence of 100 μM xanthine (solid curve) and in the absence of xanthine (broken curve). Scan rate 5 mV s^{-1}, pH 8.0, 4 °C.

the two [2Fe-2S]$^+$ centers of *R. capsulatus* XDH have been reported recently at 18 K with $g_{1,2\ 3}$ = 1.9217, 1.9217, 2.0222 for FeSI and $g_{1,2,3}$ = 1.8964, 1.9711, 2.0730 for FeSII.[32] Under the experimental conditions and concentrations employed here, the anticipated axial [2Fe-2S]$^+$ (FeSI) EPR signal emerges at relatively high temperatures but the FeSII signal is broad and barely resolvable from the other paramagnetic signals in the enzyme or the spectral baseline, even at 2 K (Figure 2, lower trace).

EPR potentiometry (pH 8.0) yielded redox potentials for the flavin cofactor of FAD/FADH (-410 ± 7 mV) and FADH/FADH$_2$ (-484 ± 7 mV) at 120 K. Plots of the experimental data points as a function of potential are shown in Figure S1 along with the theoretical curve generated by the Nernst equation for these potentials. Similarly, the Mo$^{VI/V}$ and Mo$^{V/IV}$ potentials were also determined by EPR potentiometry, with values for the Mo$^{VI/V}$ (-428 ± 10 mV) and Mo$^{VI/V}$ (-485 ± 11 mV) couples obtained. The raw data again appear in Supplementary Figure S1. At 2 K, the EPR spectrum of the FeSI center emerged, and potentiometry enabled the determination of this [2Fe-2S]$^{2+/+}$ couple to be -256 ± 10 mV. The lower potential FeSII couple could not be determined from this experiment due to the broad and weak signals that were obtained.

B. Voltammetry. Cyclic voltammetry of *R. capsulatus* XDH at pH 8 (Figure 3, unbroken curve) gives three well-separated reversible responses at low potential, with the cathodic and anodic maxima of each wave occurring at almost the same potential. This behavior is characteristic of a surface-confined electroactive species and confirmed by the observed linear dependence of the current maxima on scan rate.[33] The prominent, highest potential response (centered at -300 mV) is assigned to the overlap of three single electron couples. Supplementary Figure S3 shows that the peak width at half-height is approximately 90 mV, which is behavior typical of single electron responses.[33] The peak did not show any asymmetry and no better resolution of this multielectron wave could be obtained. The central wave also has a ca. 90 mV peak width at half-height, but is much smaller. The lowest potential maximum is distinctly asymmetric and two peaks at ca. -510
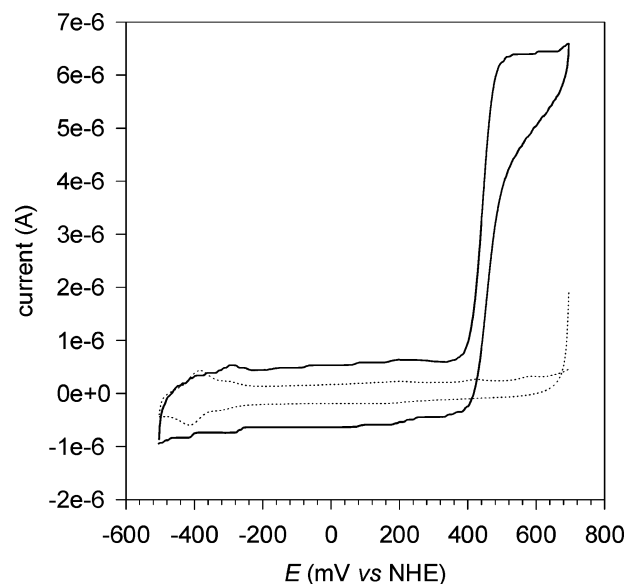
and -550 mV are apparent, with each wave exhibiting a peak width at half-height of at least 90 mV. These low potential responses are completely absent in the voltammogram of the protein where the Mo cofactor is missing (Figure 3, dotted curve).

Using the potentiometric data as a guide, we assign the highest potential response to the FeSI ([2Fe-2S]$^{2+/+}$), FAD/FADH, and FADH/FADH$_2$ couples which are not resolved in the voltammetric experiment. The two closely spaced, low potential waves (absent in the de-Moco protein voltammogram) must be the Mo$^{VI/V}$ and Mo$^{V/IV}$ couples, which leaves the small single electron wave centered at -400 mV as most likely due to the FeSII ([2Fe-2S]$^{2+/+}$) couple. Using this stoichiometry, an electrode surface coverage of 1.1 pm XDH ($\alpha\beta$-heterodimers, 35 pm cm^{-2}) was determined from the slope of the linear voltammetric sweep rate dependence of the current maxima.[33] In summary, the enzyme should be in its fully oxidized active form at ca. -200 mV and above and the onset of catalysis may be anticipated at this potential.

Catalysis. Upon addition of xanthine to the electrochemical cell, a marked increase in the anodic current from XDH is observed at ca. 400 mV (Figure 4, unbroken curve). The waveform of this voltammogram is characteristic of a catalytic electron-transfer process. The following observations indicate that the current is in fact derived from enzymatic turnover. First, no catalytic current is observed within the potential range shown in the absence of XDH, ruling out nonspecific substrate oxidation at the electrode surface. In fact, under the conditions employed here, nonspecific oxidation of xanthine does not commence until a potential of ca. 800 mV is reached (data not shown). Second, reaction with cyanide, a known inhibitor of the enzyme, results in a gradual loss of enzymatic activity. Finally, the de-Moco form of XDH, which is catalytically inactive under the same conditions, does not yield any catalytic current. These observations confirm that the enzyme is catalytically competent while immobilized on the electrode surface.

The maximum catalytic current (i_{lim}), which may be considered to be the electrochemical equivalent of reaction velocity,
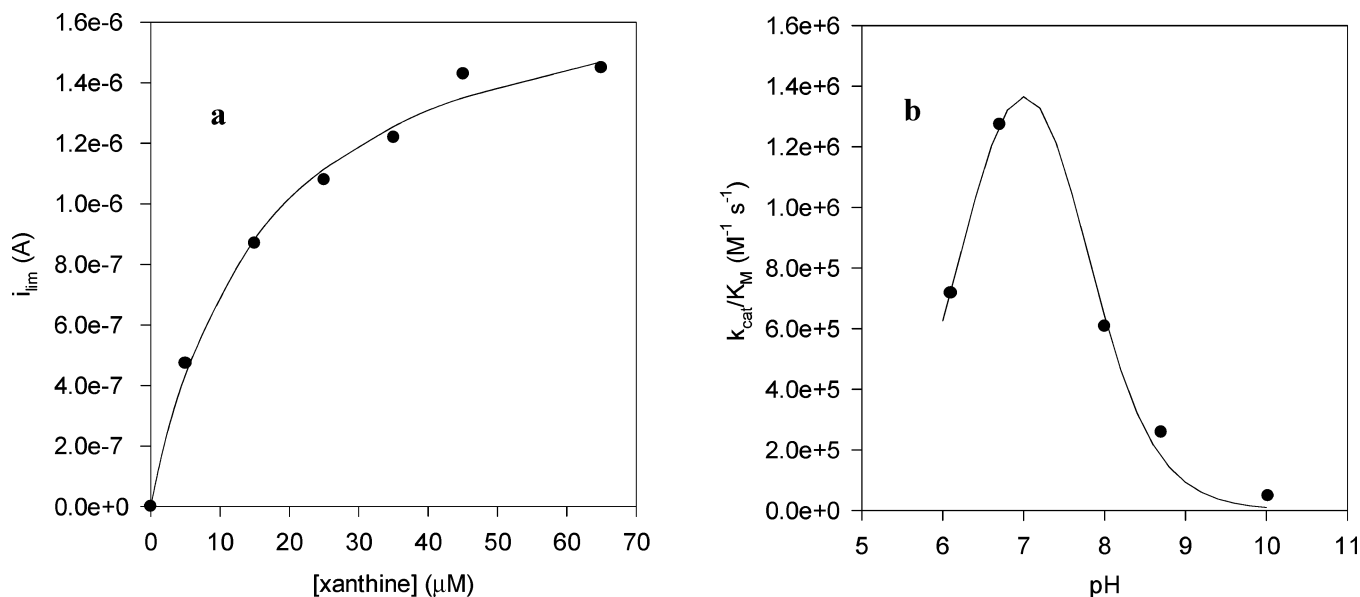
Figure 5. (a) Steady-state current (i_{lim}) as a function of xanthine concentration (pH 8.0). Solid line is a fit to the experimental points according to Michaelis—Menten kinetics. (b) k_{cat}/K_M as a function of pH ([xanthine] = 100 μM). Solid line calculated from a double ionization model with pK_a values of 6.3 and 7.7.

is dependent on (i) enzyme activity, (ii) mass transport of substrate to the protein film, and (iii) interfacial electron transfer, as described elsewhere.[38] Under ideal conditions (fast delivery of substrate under hydrodynamic conditions and effective coupling between the redox centers and the electrode surface), the latter two effects do not limit catalysis, which is only limited by enzyme activity. In this case a sigmoidal (steady state) voltammetric response is achieved. At low temperatures (4 °C, Figure 4) we indeed found this to be the case, but at 25 °C, peak-shaped curves were seen (Figure S4) reflecting substrate depletion within the (substrate) diffusion layer (transient voltammetric behavior). Although the peak currents will approach the ideal (enzyme limited) steady state current, they will be necessarily smaller (limited by mass transport) and the apparent values of k_{cat} represent lower bounds to the true enzyme activity. Nevertheless, it is assumed that the observed peak currents (as a function of substrate concentration) are proportional (but not equal to) to the ideal enzyme limited currents. On the basis of the preliminary temperature-dependent data that we have, at low temperature enzyme activity is attenuated sufficiently such that mass transport is not limiting, but at room temperature enzyme activity exceeds the rate of substrate delivery to the active site. Variable temperature hydrodynamic experiments (rotating disk voltammetry) may provide more information on the interplay between these two factors in limiting catalysis.

The apparent limiting currents at 25 °C followed Michaelis—Menten kinetics (Figure 5a) across the range pH 6 to 10. Importantly, the potential at which catalysis begins is essentially independent of substrate concentration (see Supplementary Figure S4). From the calculated surface coverage of the enzyme (1.1 pm), and the 2-electron stoichiometry of the catalytic reaction, k_{cat} for XDH immobilized on the electrode surface was determined at each pH value. Values of K_M and k_{cat} are as follows: pH 6.1 (23 μM and 16 s^{-1}); pH 6.7 (20 μM and 25 s^{-1}); pH 8.0 (15 μM and 9 s^{-1}); pH 8.7 (54 μM and 13 s^{-1}); and pH 10.0 (62 μM and 3 s^{-1}).

A plot of k_{cat}/K_M (the effective second-order rate constant for the catalytic reaction at low substrate concentrations[39]) within the range 6 < pH < 10 appears in Figure 5b, where a distinctly bell-shaped profile is seen, with a pH optimum of 7.0. The solid curve in Figure 5b represents the calculated pH dependence for a double ionization model[39] where the active enzyme/substrate system must be in its intermediate (singly protonated) form employing pK_a values of 6.3 and 7.7.

Discussion

As electron transfer is central to the function of XDH, an examination of the redox potentials of the four cofactors is pertinent. During turnover, xanthine donates two electrons to the fully oxidized Mo^{VI} active site. Ultimately, the FAD cofactor is the terminus at which electrons are transferred to the NAD$^+$ acceptor. However, the potentials shown in Table 1 demonstrate that the four cofactors, defined in the crystal structure of *R. capsulatus* XDH (see Supplementary Figure S5), are not arranged sequentially in order of their redox potentials, i.e., from highest to lowest potential. In contrast to bovine XO[40] and other xanthine oxidoreductases (Table 1), in *R. capsulatus* XDH the highest potential center (FeSI) lies closest to the lowest potential Mo cofactor. Instead, equilibration of reducing equivalents occurs across the six possible "holes" provided by the four cofactors, as has been shown previously for the bovine enzyme using time-resolved spectroscopic and stopped-flow techniques.[41]

Examination of XDH by EPR as a function of potential and temperature enabled the observation of signals attributable to the paramagnetic FADH, Mo^V, and reduced [2Fe-2S]$^+$ centers. FeSI, which lies closest to the Mo-center, has axial symmetry

(38) Heering, H. A.; Hirst, J.; Armstrong, F. A. *J. Phys. Chem. B* **1998**, *102*, 6889—6902.

(39) Kim, J. H.; Ryan, M. G.; Knaut, H.; Hille, R. *J. Biol. Chem.* **1996**, *271*, 6771—6780.

(40) Hille, R.; Anderson, R. F. *J. Biol. Chem.* **2001**, *276*, 31193—31201.

(41) Olson, J. S.; Ballou, D. P.; Palmer, G.; Massey, V. *J. Biol. Chem.* **1974**, *249*, 4350—4362.

Table 1. Redox Potentials (mV vs NHE) for Selected Xanthine Oxidoreductases (potentials in italics from cyclic voltammetry, all others from potentiometry)

	origin	pH	FAD/FADH	FADH/FADH$_2$	FeSI	FeSII	Mo$^{VI/V}$	Mo$^{V/IV}$	ref
XDH	*R. capsulatus*	8.0	−410	−484	−256	n.d.	−421	−499	this work
		8.0	*−300*	*−300*	*−300*	*−400*	*−510*	*−540*	this work
XDH	*P. putida*	8.0	−350	−350	−335	n.d.	−360	−300	20
XDH	bovine milk	7.5	−270	−410	−310	−235	n.d.	n.d.	19
XDH	chicken liver	7.8	−345	−377	−280	−275	−357	−337	15
XDH	turkey liver	8.2	−359	−362	−295	−292	−350	−362	14
XO	bovine milk	7.7	−332	−234	−310	−255	−373	−377	17

(*g* values 1.922 and 2.022)[32] and was identified in our EPR potentiometric titration to have the highest redox potential. The axial EPR spectrum of this cluster is unusual, as the signal from this center in other members of the XO family generally show rhombic symmetry. In *R. capsulatus* XDH the low-potential cluster, FeSII, is situated closer to the FAD cofactor and exhibits a particularly broadened, rhombic EPR spectrum that is only developed at low temperatures (*g* values 1.896, 1.971, and 2.073).[32] It was not possible to obtain a reliable value of its reduction potential from our EPR experiments.

Cyclic voltammetry could not provide clear resolution of all six oxidation−reduction couples. However, three distinct couples were observed (Figure 3) at potentials comparable with those found by potentiometry. The most intense signal is consistent with an overlap of the two FAD couples and that for the higher potential FeSI center. The broad, lowest potential wave is assigned to the Mo cofactor. This represents only the third example of a nonturnover voltammetric response from the active site of a mononuclear Mo enzyme.[29,30] The small reversible wave found at −400 mV is attributed to the lower potential FeSII cluster.

The redox potentials determined here may be compared with those reported for other members of the XO family (Table 1). Although there is no clear trend in the potentials for the enzymes listed in this table, some important features emerge from the present study. First, the well-separated FAD potentials for *R. capsulatus* XDH result in the FADH semiquinone being stable over a broad potential range, and this has been found to be a distinguishing feature of XDH as opposed to XO enzymes. Furthermore, the relatively low potential FAD couples dictate that the reduced flavin is well poised to deliver electrons efficiently to the NAD$^+$ cofactor ($E°$ −335 mV, pH 7.5) during turnover. The flavin potentials have been suggested to be a factor in determining the dehydrogenase or oxidase activity of the enzyme; where high potentials favor oxidase activity. However, the situation is more complicated than this. NAD$^+$ binding studies[42] and crystallography[6] have shown that access to the putative NAD$^+$ binding site adjacent to the FAD moiety is affected by the XDH to XO conversion.

The well-separated Mo$^{VI/V}$ and Mo$^{V/IV}$ couples also enabled a clear identification of the paramagnetic Mo^V oxidation state using EPR spectroscopy. The classical "rapid" type I EPR spectrum of the Mo^V cofactor is very similar to that seen in other XDH and XO analogues. A second notable feature is the particularly negative Mo potentials, which are, to our knowledge, the lowest yet seen for a mononuclear Mo enzyme.

Clearly there are significant differences between the redox potentials determined voltammetrically and those obtained from the EPR titration. There are many reasons that might account for this disparity. The voltammetric experiment requires the protein to be confined to the electrode surface, and conformational changes upon adsorption may result in different apparent redox potentials. One would expect this to be most significant in solvent exposed cofactors (close to the surface of the protein), more so than with cofactors buried well within the protein. Also, protein voltammetry, unlike redox potentiometry, is performed without mediators and interactions between the mediators and the cofactors may also influence the observed potentials. Finally, it is apparent that voltammetry does not offer the excellent resolution of different redox centers provided by EPR potentiometry. Despite the FAD, 2Fe-2S clusters, and Mo centers exhibiting quite similar potentials, their well-separated EPR signals (as both a function of field position and temperature) enabled their clear resolution. Considerable overlap was seen in the corresponding voltammetry experiment, as all responses can only be resolved in the potential domain.

The catalytic current seen upon addition of xanthine is indicative of electrochemically driven enzyme turnover. The pH-dependence of the electrochemically determined of k_{cat}/K_M ratio mirrors that reported by Hille and co-workers who reported a very similar bell-shaped pH dependence of k_{cat}/K_M for bovine milk XO (pK_a values of 6.6 and 7.4).[39] The higher pK_a was assigned to deprotonation of xanthine, while the lower pK_a was initially suggested to involve protonation of the terminal sulfido ligand in the Mo^{VI} form, although a more recent proposal[43] favors protonation of a glutamate residue situated beneath the square pyramidal Mo cofactor. The carboxylate side chain is postulated to act as a proton acceptor during nucleophilic attack by the equatorial hydroxo ligand on the substrate xanthine.[43] In *R. capsulatus* XDH this glutamate (E730) is conserved and occupies a similar position relative to the active site,[11] so the same model may be applied in this case. In passing, we note that performing similar electrochemical experiments in a solution buffered at pH 8.0 with Tris, as opposed to a buffer mixture of bis-tris propane and 2-amino-2-methylpropan-1-ol, resulted in a much-increased value of K_M (480 μM). No significant inhibition due to Tris buffer has been seen in solution assays of XDH, and our observations may be specific to the protein film voltammetry experiment. Further studies are required to clarify this point.

A key issue is the potential at which electrochemically driven catalysis begins. In principle, at potentials positive of −200 mV, all redox-active centers in XDH are fully oxidized and hence the enzyme should be catalytically active. However, catalysis does not begin until the electrode potential reaches ca. +400 mV. Differential binding of the substrate to its fully oxidized

(42) Harris, C. M.; Massey, V. *J. Biol. Chem.* **1997**, *272*, 28335−28341.

(43) Xia, M.; Dempski, R.; Hille, R. *J. Biol. Chem.* **1999**, *274*, 3323−3330.

Scheme 1

inactive

active
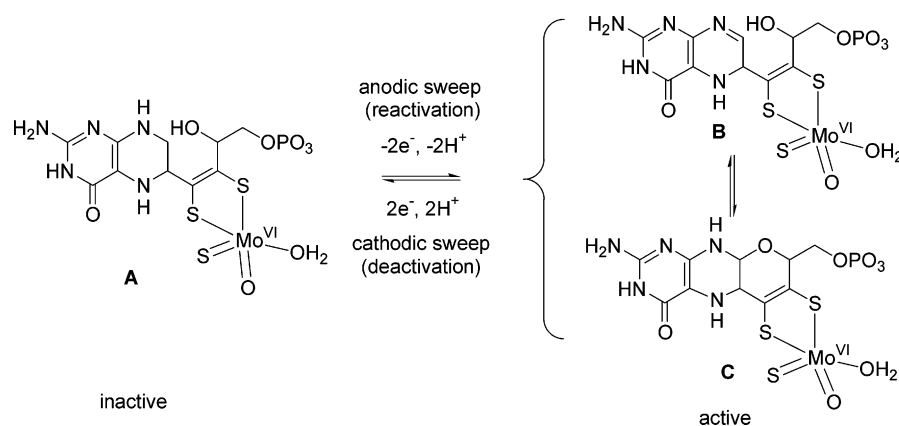
and reduced forms is expected to influence the potential at which catalysis occurs,[38] but we see no variation in the catalytic potential at either low or high substrate concentrations.

This conundrum can be rationalized if the enzyme is undergoing a reversible reductive (de)activation at a potential well positive of its cofactors during voltammetry and requires oxidative (re)activation to restore catalytic activity. Our hypothesis is that the pterin ring is the site of oxidation. In all crystal structures of mononuclear Mo enzymes determined to date, the pyranopterin is bound to the metal as form **C** shown in Scheme 1. This tricyclic structure is related by a reversible ring opening reaction to the unsaturated alcohol form (**B**). This unsaturated alcohol-appended pterin may be reduced to the ring-opened tetrahydropterin analogue (**A**), which is now incapable of undergoing ring closure. Indeed this ring-opened tetrahydropterin state is the form that has been isolated in degradation studies.[44] We propose that a similar series of transformations is occurring to the coordinated pterin during voltammetry, i.e., on the cathodic sweep, the pterin is reduced to the ring-opened tetrahydro form (**A**), which is catalytically inactive, and that oxidative dehydrogenation (at 400 mV) is necessary to restore activity to its tricyclic form (**C**).

A precedent for such a mechanism exists in a study of mutant strains of *Drosophila melanogaster* XDH.[45] One particular mutant from this investigation (G1011E) was activated following mild oxidation with phenazine methosulfate. It was proposed that the pterin-dithiolene ligand was incorporated into the enzyme in its ring-opened fully reduced form (**A**). In various voltammetric investigations of the oxidative dehydrogenation of substituted tetrahydropterins[46-48] this occurs at ca. +150 mV, and being coordinated to the molybdenum should raise this potential further. Importantly, there is no hysteresis. The potential at which catalysis ceases on the cathodic sweep is evidently the same as that seen on the anodic sweep.

A transformation such as that shown in Scheme 1 could bring about major conformational changes at the active site. In its ring-opened form, the pterin-dithiolene ligand has greater conformational flexibility and may uncouple electron transfer

between molybdenum and the adjacent 2Fe-2S cofactor to the point that electron egress from the active site is disabled and turnover ceases, i.e., the oxidative half reaction then becomes rate limiting. Although resolution of the voltammetrically determined potentials of XDH (of the putative "hyper-reduced" form) was not as clear as those obtained potentiometrically, their similarities suggest that any electrochemically induced, ligand centered oxidation–reduction processes do not have a marked effect of the reduction potentials of the cofactors.

Our model involving pterin oxidation as a switch of catalytic activity is novel and represents a significant finding which may be relevant to the electrochemistry of other mononuclear Mo enzymes, all of which contain the pterin-dithiolene cofactor. Under physiological conditions, the main reductants that XDH encounters are hypoxanthine, xanthine and other purines, pyridines, and pteridines in addition to various aromatic and aliphatic aldehydes. These molecules are specific reductants of the Mo^{VI} active site, but no other center within the enzyme. The two electrons delivered by the substrate, e.g., xanthine, to the Mo active site equilibrate among the higher potential FAD and [2Fe-2S] centers, and no ligand-centered reduction of the pterin is likely. During the cathodic voltammetric sweep, the enzyme has access to a large source of electrons, which may be delivered to it at a greater rate than would occur in vivo, thus enabling nonphysiologically relevant transformations to take place. We are currently investigating further the electrochemistry of other mononuclear Mo enzymes in an effort to better understand their complex and interesting reactivity.

Supporting Information Available: EPR spectra as a function of potential at 120 K (Figure S1) and 2 K (Figure S2), expansion of anodic nonturnover voltammetric waves for XDH (Figure S3), catalytic voltammetry of XDH at 25 °C (Figure S4), and a view of the four redox centers in XDH taken from the published crystal structure (Figure S5). This material is available free of charge via the Internet at http://pubs.acs.org.

JA037940E

(44) Rajagopalan, K. V.; Johnson, J. L. *J. Biol. Chem.* **1992**, *267*, 10199−10202.
(45) Doyle, W. A.; Burke, J. F.; Chovnick, A.; Dutton, F. L.; Whittle, J. R. S.; Bray, R. C. *Eur. J. Biochem.* **1996**, *239*, 782−795.
(46) Raghavan, R.; Dryhurst, G. *J. Electroanal. Chem. Interfacial Electrochem.* **1981**, *129*, 189−212.
(47) Ege-Serpkenci, D.; Dryhurst, G. *Bioelectrochem. Bioenerg.* **1983**, *11*, 51−59.
(48) Ege-Serpkenci, D.; Raghavan, R.; Dryhurst, G. *Bioelectrochem. Bioenerg.* **1983**, *10*, 357−376.